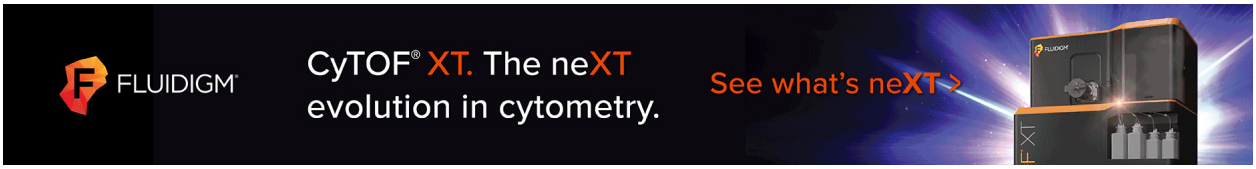

The Journal of Immunology

Insights into the Mechanism of Action of Highly Diluted Biologics

Sergey A. Tarasov, Evgeniy A. Gorbunov, Elena S. Don, Alexandra G. Emelyanova, Alexander L. Kovalchuk, Naveena Yanamala, A. Sylvia S. Schleker, Judith Klein-Seetharaman, Reno Groenestein, Jean-Pierre Tafani, Peter van der Meide and Oleg I. Epstein

J Immunol 2020; 205:1345-1354; Prepublished online 29 July 2020;
doi: 10.4049/jimmunol.2000098
http://www.jimmunol.org/content/205/5/1345

This information is current as of October 10, 2021.

Supplementary Material **http://www.jimmunol.org/content/suppl/2020/07/28/jimmunol.2000098.DCSupplemental**

References This article **cites 62 articles**, 11 of which you can access for free at:
http://www.jimmunol.org/content/205/5/1345.full#ref-list-1

Why *The JI*? Submit online.

- **Rapid Reviews! 30 days*** from submission to initial decision
- **No Triage!** Every submission reviewed by practicing scientists
- **Fast Publication!** 4 weeks from acceptance to publication

**average*

Subscription Information about subscribing to *The Journal of Immunology* is online at:
http://jimmunol.org/subscription

Permissions Submit copyright permission requests at:
http://www.aai.org/About/Publications/JI/copyright.html

Email Alerts Receive free email-alerts when new articles cite this article. Sign up at:
http://jimmunol.org/alerts

The Journal of Immunology is published twice each month by
The American Association of Immunologists, Inc.,
1451 Rockville Pike, Suite 650, Rockville, MD 20852
Copyright © 2020 by The American Association of Immunologists, Inc. All rights reserved.
Print ISSN: 0022-1767 Online ISSN: 1550-6606.

Downloaded from http://www.jimmunol.org/ by guest on October 10, 2021

Insights into the Mechanism of Action of Highly Diluted Biologics

Sergey A. Tarasov,*,† Evgeniy A. Gorbunov,* Elena S. Don,*,† Alexandra G. Emelyanova,*,† Alexander L. Kovalchuk,* Naveena Yanamala,‡ A. Sylvia S. Schleker,‡ Judith Klein-Seetharaman,‡ Reno Groenestein,§ Jean-Pierre Tafani,¶ Peter van der Meide,§ and Oleg I. Epstein*,†

The therapeutic use of Abs in cancer, autoimmunity, transplantation, and other fields is among the major biopharmaceutical advances of the 20th century. Broader use of Ab-based drugs is constrained because of their high production costs and frequent side effects. One promising approach to overcome these limitations is the use of highly diluted Abs, which are produced by gradual reduction of an Ab concentration to an extremely low level. This technology was used to create a group of drugs for the treatment of various diseases, depending on the specificity of the used Abs. Highly diluted Abs to IFN-γ (hd-anti–IFN-γ) have been demonstrated to be efficacious against influenza and other respiratory infections in a variety of preclinical and clinical studies. In the current study, we provide evidence for a possible mechanism of action of hd-anti–IFN-γ. Using high-resolution solution nuclear magnetic resonance spectroscopy, we show that the drug induced conformational changes in the IFN-γ molecule. Chemical shift changes occurred in the amino acids located primarily at the dimer interface and at the C-terminal region of IFN-γ. These molecular changes could be crucial for the function of the protein, as evidenced by an observed hd-anti–IFN-γ–induced increase in the specific binding of IFN-γ to its receptor in U937 cells, enhanced induced production of IFN-γ in human PBMC culture, and increased survival of influenza A–infected mice. ***The Journal of Immunology*****, 2020, 205: 1345–1354.**

Antibody-based drugs are rapidly expanding their share of the medicinal product market. Approximately 60 mAbs have been approved for clinical use (1). Despite the increasing demand, the use of therapeutic Abs remains to be challenging because of the limitations in their oral availability, problems with stability, and their side effects (2, 3). Therefore, many studies have been aimed at designing and augmenting the Ab-based pharmaceuticals through adjuvants, chemical modifications, encapsulation, etc. (4–6).

One of the promising novel approaches to overcome those limitations is a gradual decrease of the original Ab concentration to achieve its ultra-high dilution (7). This platform has successfully been used for manufacturing a group of safe and efficacious drugs for the treatment of various conditions, including infectious diseases, endocrine disorders, urogenital dysfunction, etc. (8–10).

The abovementioned technology was applied to target regulatory molecules, including cytokine IFN-γ that is involved in various physiological and disease states. IFN-γ is a homodimeric glycoprotein (Fig. 1) with pleiotropic functions produced primarily by T lymphocytes and NK cells. It acts as a modulator of plethora of immune functions, including antiviral immune response. IFN-γ exerts these activities through binding to its high-affinity receptor that consists of α- and β-chains, leading to their association into an active complex and signaling via the JAK/STAT pathway (11).

Abs against IFN-γ have been used to affect the immune response in experimental models (12, 13), but their clinical development was unsuccessful despite demonstrating some benefits (14, 15). Naturally occurring autoantibodies to IFN-γ are present in healthy individuals; they increase in titer during infections and in some diseases, and they were shown to interfere with the immunomodulatory activity of the cytokine (16). These facts prompted us to consider Ab-based approach to modulate IFN-γ functions in vivo by developing an agent based on the highly diluted Abs to IFN-γ (hd-anti–IFN-γ). To date, the ability of the hd-anti–IFN-γ to regulate functional activity and production of endogenous IFNs, modulate the immune response, and affect the level of natural circulating Abs to IFN-γ has already been studied (17, 18). Also, the antiviral activity of the hd-anti–IFN-γ against influenza and other respiratory infections has been demonstrated in a variety of preclinical and clinical studies (17, 19–23). Information regarding recent clinical trials can be found on ClinicalTrials.gov (https://clinicaltrials.gov/ct2/results?cond=&term=anaferon&cntry=&state=&city=&dist=).

Physicochemical properties of the hd-anti–IFN-γ have been studied by dynamic light scattering, conductometry, pH meters, and tensiometry. These results have demonstrated that aqueous solutions of highly diluted Abs are self-organizing, dispersed

*OOO "NPF "Materia Medica Holding," 127473 Moscow, Russian Federation; †The Institute of General Pathology and Pathophysiology, 125315 Moscow, Russian Federation; ‡Department of Structural Biology, University of Pittsburgh School of Medicine, Pittsburgh, PA 15260; §U-CyTech biosciences, 3584 CM Utrecht, the Netherlands; and ¶Apcis, 94700 Maisons Alfort, France

ORCID: 0000-0001-7547-1008 (E.A.G.).

Received for publication January 29, 2020. Accepted for publication July 4, 2020.

This work was supported by OOO "NPF "Materia Medica Holding," Moscow, Russian Federation.

The employees of OOO "NPF "Materia Medica Holding" took part in the design of the experiments and the manuscript writing, performed statistical analysis, and made a decision to publish the work.

Address correspondence and reprint requests to Dr. Evgeniy A. Gorbunov, OOO "NPF "Materia Medica Holding," 3rd Samotyochny Pereulok, 9, 127473 Moscow, Russian Federation. E-mail address: GorbunovEA@materiamedica.ru

The online version of this article contains supplemental material.

Abbreviations used in this article: 1D, one-dimensional; 2D, two-dimensional; hd-anti–IFN-γ, highly diluted Ab to IFN-γ; hd-anti–TNF-α, highly diluted Ab to TNF-α; HSQC, heteronuclear single quantum coherence; IFNGR1, IFN-γ receptor 1; NMR, nuclear magnetic resonance.

Copyright © 2020 by The American Association of Immunologists, Inc. 0022-1767/20/$37.50

Downloaded from http://www.jimmunol.org/ by guest on October 10, 2021

systems in which nano-objects are formed (24). Self-organization of Ab solutions was accompanied by a significant change in their properties as compared with similarly treated water. Additionally, it was shown that solution of the hd-anti–IFN-γ might contain aggregates of initial Abs associated with gas nanobubbles, which remain in a multiple times–diluted liquid because of the flotation effect (25). These data agree with the previously demonstrated presence of the starting materials in nanoparticulate form even in the extreme dilutions (26).

Using piezoelectric immunosensor assay, we have shown that the interaction between IFN-γ and IFN-γ–specific Abs changed in the presence of the hd-anti–IFN-γ (27). Conformational changes of an Ag upon binding of an Ab have been demonstrated (28). Similar allosteric effect on an Ag may also be attributed to highly diluted Abs. Thus, the aim of the current study was to investigate whether the hd-anti–IFN-γ may cause a conformational change in IFN-γ molecule, affecting its biological activity and interaction with other molecules (i.e., IFN-γ receptor).

Materials and Methods

Production of experimental samples

The hd-anti–IFN-γ is an active pharmaceutical ingredient of an antiviral commercial drug Anaferon for Children (OOO "NPF "Materia Medica Holding," Moscow, Russian Federation). Affinity-purified rabbit polyclonal Abs to human rIFN-γ (stock concentration 2.5 mg/ml) were manufactured in accordance with the current European Union requirements for GMP for starting materials (29) by Angel Biotechnology Holdings (Penicuik, U.K.). The hd-anti–IFN-γ were produced by the GMP manufacturing facility of OOO "NPF "Materia Medica Holding," according to the technology described in the United States patent 8,535,664 (30). Briefly, Abs to IFN-γ (2.5 mg/ml) were mixed with a solvent (ethanol–water solution) at a ratio of 1:100 and underwent intensive vibration treatment to produce the first centesimal dilution (i.e., 100-fold dilution). All subsequent dilutions comprised one part of the previous dilution and 99 parts of solvent (ethanol–water solution for intermediate dilutions and purified water for the preparation of the final dilutions), with intensive vibration treatment between the dilution steps. Finally, the hd-anti–IFN-γ contain the mixture of 12th, 30th, and 50th centesimal dilutions. The theoretical concentration reduction level of the original Abs is 1×10^{24} at least. Thus, if we do not take into account the physical aspects mentioned in the *Introduction*, the theoretical concentration of initial Abs might be 2.5×10^{-24} mg/ml. This value is mentioned in this article only to avoid misunderstanding regarding the dilution level. The highly diluted Abs to TNF-α (hd-anti–TNF-α) were prepared using a similar method, but the starting solution contained affinity-purified rabbit polyclonal Abs against human rTNF-α (stock concentration 2.5 mg/ml). The placebo control containing no Abs was prepared by applying identical procedure to purified water. The purified water was used as vehicle. All solutions were prepared in glass vials under sterile conditions protected from direct intense light and were stored at room temperature. The samples were coded by manufacturer and sent to research organizations in the United States (University of Pittsburgh), Belgium (Euroscreen), the Netherlands (U-CyTech biosciences), and France (Apcis), where the corresponding studies were conducted independently. The samples were tested blindly.

Nuclear magnetic resonance spectroscopy

The coding sequence for human IFN-γ without signal peptide (Thermo Fisher Scientific) was cloned in frame with an N-terminal His6-tag, followed by a Strep-tag into the pET-28b(+) vector (Novagen). IFN-γ was amplified from cDNA in a two-step PCR using three primers (forward primer 1: 5′-CCGCAGTTCGAAAAAGGCGCGCCC**CAGGACCCATATGTGTA**-3′; 5′–forward primer 2: 5′-TATACATATGG*CTAGC*TGGAGCCACCCGCAGTTCGAAAAA-3′; reverse primer: 5′-GTG*CTAG*TCGACGC *GGCC*G**CTTACTGGGATGCTCTTCG**-3′) to obtain a fragment introducing the Strep-tag as well as the restriction sites NheI and NotI required for cloning into the pET-28(b+) vector. The complete construct was transformed into Rosetta(DE3)pLysS competent cells (Lucigen). Double yeast tryptone medium (16 g tryptone, 10 g yeast extract, and 5 g NaCl per liter [pH 7.4]) containing 50 μg/ml kanamycin was inoculated with a glycerol stock of recombinant cells and incubated overnight at 37°C with shaking (200 rpm). One liter of the double yeast tryptone medium with 50 μg/ml kanamycin was inoculated with the overnight culture to obtain a starting OD_{600} of 0.1. The culture was split equally into three 2-l flasks and incubated at 37°C with shaking at 160 rpm until reaching an OD_{600} of 0.5–0.6. The cells were harvested by centrifugation (3000 × *g*; 30 min), and the supernatant was removed. Each pellet was resuspended in 0.3 l M9 minimal medium (6.6 g Na_2HPO_4, 3.0 g KH_2PO_4, 0.5 g NaCl, 0.4% glucose, 1.0 mM $MgSO_4$, 0.1 mM $CaCl_2$, 1.0 mg biotin, and 0.5 mg thiamine/l) supplemented with 1.0 g/l ^{15}N-labeled NH_4Cl (Cambridge Isotopes) containing 50 μg/ml kanamycin and incubated at 37°C with shaking at 160 rpm for 1 h. Expression was induced by adding isopropyl β-D-1-thiogalactopyranoside to a final concentration of 1.0 mM, and the culture was incubated for 4 h at 37°C with shaking at 160 rpm. The cells were harvested by centrifugation, and the pellet was frozen at −20°C.

The pellet was then thawed and resuspended in 5 ml of buffer A (50 mM sodium phosphate [pH 8] and 300 mM NaCl) per 1.0 g of fresh weight. The suspension was sonicated using six pulses of 10 s each, with a 10-s pause on ice in between the pulses. The lysate was centrifuged at 5000 × *g* at 4°C for 15 min, and the pellet was further resuspended in the same amount of buffer A. Following the centrifugation step at 5000 × *g* at 4°C for 15 min, the pellet was resuspended in 5 ml of buffer B (100 mM sodium phosphate [pH 8], 10 mM Tris, and 6.0 M guanidine hydrochloride) per 1.0 g fresh weight of pellet and stirred for 1 h at room temperature. The suspension was centrifuged at 15,000 × *g* for 30 min at 4°C, and the supernatant was loaded onto a 5-ml Ni-NTA column (QIAGEN) that had been equilibrated with five column volumes of buffer B. The column was washed with 10 column volumes of buffer B and 10 column volumes of buffer C (100 mM sodium phosphate [pH 6.3], 10 mM Tris, and 6.0 M guanidine hydrochloride) before eluting the protein with four column volumes of elution buffer (100 mM sodium phosphate buffer [pH 4.5], 10 mM Tris, and 6.0 M guanidine hydrochloride). In total, 350 ml of refolding buffer (150 mM NaCl, 100 mM glycine, 20 mM Tris [pH 8], 100 mM PMSF, and one protease inhibitor tablet [catalog no. 04693132001; Roche]) were added dropwise to the elution fractions at room temperature while stirring to promote refolding of the protein. Subsequently, the solution was left at 4°C overnight under constant stirring. The following day, the solution was concentrated using a filter device (10 kDa cutoff) to a volume of ∼5 ml. The concentrated protein was loaded onto a Superdex 75 (16/60) gel filtration column after equilibrating the column with 120 ml of gel filtration buffer (10 mM sodium phosphate buffer [pH 7.4], 150 mM NaCl, and one protease inhibitor tablet). The loop was washed with 15 ml of gel filtration buffer, and the sample was eluted at a flow rate of 1.0 ml/min with 1.5 column volumes of the same buffer into 2.0-ml elution fractions. The eluted fractions containing the ^{15}N-labeled IFN-γ were pooled and concentrated to 0.4 mM using Amicon concentrators for nuclear magnetic resonance (NMR) studies, and were analyzed at the final concentration of 50 μM.

The NMR experiments were performed at 25°C on a Bruker Avance 900 MHz spectrometer equipped with a 5-mm, triple resonance, and *z*-axis gradient cryoprobe. The two-dimensional (2D) ^1H–^{15}N spectra for IFN-γ alone were acquired using a standard heteronuclear single quantum coherence (HSQC) pulse sequence with 128 scans in the proton dimension and 128 scans in the nitrogen dimension, with a delay of 1 s. For NMR samples containing IFN-γ with added highly diluted Abs or placebo, spectra were acquired with 2048 × 34 scans. Data acquisition was performed using TopSpin version 3.0 software (Bruker BioSpin, Billerica, MA). The spectra were processed and analyzed using NMR View (31) and Sparky software (SPARKY 3; from T. D. Goddard and D. G. Kneller, University of California, San Francisco). The observed backbone resonances were assigned using previously published NMR data that were acquired under similar conditions for an IFN-γ construct containing residues 1–133 (of 143 total residues) (32). Of the 133 expected backbone amide signals, 130 were observed in the HSQC spectrum. We unambiguously assigned 128 of the 130 previously assigned residues in our sample. For assignment purposes, a more highly concentrated sample than that used for testing the effects of hd-anti–IFN-γ was prepared and subjected to 2D ^1H–^{15}N HSQC spectroscopic analysis. This sample contained 400 μM concentrated ^{15}N-labeled IFN-γ in 20 mM potassium phosphate buffer (pH 6) containing 20 mM NaCl and 10% D_2O, which was used to record spectra. For the NMR experiments involving the hd-anti–IFN-γ and placebo, the test samples were added to 50 μM ^{15}N-labeled IFN-γ in 20 mM potassium phosphate buffer (pH 6), 20 mM NaCl, and 10% D_2O. In each case, the NMR samples were prepared in an identical fashion in three separate tubes: 21.5 μl of IFN-γ plus 113 μl of buffer (20 mM K_2HPO_4/KH_2PO_4 plus 20 mM NaCl plus 10%D_2O, [pH 6]) was added to 42 μl of either placebo or hd-anti–IFN-γ to give a final concentration of 50 μM IFN-γ.

Radioligand binding saturation assay

The assay was performed by adding the following reagents successively to siliconized microcentrifuge tubes: 50 μl of assay buffer (RPMI 1640

Downloaded from http://www.jimmunol.org/ by guest on October 10, 2021

culture medium [12–115F; Lonza Bioscience] supplemented with 10% FBS [CH30160.03; Perbio]), 25 μl of [^{125}I]IFN-γ (diluted in assay buffer with 0.4% sodium azide at increasing concentrations [3.0, 1.0, 0.3, 0.1, 0.03, 0.01, 0.003, and 0.001 nM; 285-IF/CF; R&D Systems; custom-labeling by Perkin Elmer]), and 25 μl of human monocyte-like cell line U-937 suspension (85011440; Sigma-Aldrich; 1 million cells per tube, diluted in assay buffer without sodium azide; 200 μg of total protein per data point). To determine nonspecific binding 50 μl of IFN-γ (285-IF/CF; R&D Systems) (diluted in assay buffer without sodium azide to reach a 300-nM final concentration) was added to the well instead of 50 μl of assay buffer.

The tubes were incubated for 150 min at 4°C and then centrifuged. The supernatant was removed, and the cell pellets were washed once with 1 ml of ice-cold assay buffer. The tubes were centrifuged again, the supernatant was removed, and the bottom of the tube containing the cell pellet was cut, placed in counting tubes, and then counted with a Cobra Gamma Counter (Packard Instrument) for 1 min/tube.

The *Kd* values were calculated using GraphPad Prism software and the one-site binding (hyperbola) option. Dose-response data were analyzed with XLfit software (IDBS Software Solutions) using nonlinear regression applied to a sigmoidal dose-response model as described in the respective GraphPad guide to analyzing radioligand binding data (33).

Radioligand binding competition assay

The assay was performed by adding successively the following reagents in siliconized microcentrifuge tubes: 50 μl of either hd-anti–IFN-γ ($n = 5$), hd-anti–TNF-α ($n = 5$), vehicle ($n = 4$), buffer ($n = 3$) (assay buffer without sodium azide), or IFN-γ (diluted in assay buffer without sodium azide) at increasing concentrations (0.001, 0.01, 0.1, 1.0, 10, and 100 nM), 25 μl of [^{125}I]IFN-γ (diluted in the assay buffer with 0.4% sodium azide at the concentration corresponding to the $Kd = 0.14 \pm 0.05$ nM, as determined by the radioligand saturation binding assay; Supplemental Fig. 1), and 25 μl of U-937 cell suspension (1 million cells per tube, diluted in assay buffer without sodium azide; 200 μg of a total protein per data point in case of determination of total ligand binding). The following procedure is the same as for the saturation binding assay.

An IFN-γ ELISpot assay

A human IFN-γ ELISpot Kit (red spot; catalog no. CT230-PR2; U-CyTech biosciences) was used to determine the effect of the hd-anti–IFN-γ or vehicle on the generation of IFN-γ–producing cells in the population of 4×10^5 human PBMCs per well with standard cell stimulus. PBMC were isolated from venous blood of a single healthy donor by density gradient centrifugation. The procedure was performed according to the manufacturer's instructions, with a few modifications. Briefly, PVDF membrane-bottom plates were prewetted and coated with capture Ab overnight at 4°C. Before starting the experiment, the culture medium was lyophilized (duration 48 h). The dry substance was subsequently reconstituted in the hd-anti–IFN-γ ($n = 6$) or vehicle ($n = 6$) and then filter sterilized (0.2 μm). U-CyTech biosciences (Utrecht, the Netherlands) provided human PBMCs. The cells were resuspended in culture medium containing the hd-anti–IFN-γ or vehicle and stimulated with the ICE Peptide Pool (a pool of 23 viral peptides of influenza A virus, CMV, and EBV epitopes recognized by CD8$^+$ T cells, catalog no. CT370; U-CyTech biosciences). The wells with unstimulated cells in medium reconstituted in vehicle were used as control for background spot counts.

PBMC were seeded at 4×10^5 cells per well in 100 μl in triplicate. ELISpot plates were covered with lids and incubated at 37°C, 5% CO_2, and 100% humidity for ∼20 h. After the incubation and washing, the bulk of the cells was removed with a firm shakeout action, and biotinylated detection Abs were added to each well for 1 h at 37°C. Further, streptavidin–HRP solution was added into the wells for 1 h at 37°C, followed by 3-amino-9-ethylcarbazole substrate yielding a colored zone (spot) for 25 min at room temperature. Color development was stopped by thoroughly rinsing both sides of the PVDF membrane with demineralized water (produced in house), and plates were air dried at room temperature. The colored zone reveals the site of cytokine secretion, and IFN-γ–producing cells were enumerated by analyzing the color development with an ImmunoSpot Image Analyzer (CTL, Oberndorf am Neckar, Germany).

Animals and in vivo experiments

Mice. In the study with H1N1 virus, 4–5-wk-old, 15–17-g (at viral challenge), female BALB/c mice (Janvier Labs, Le Genest-Saint-Isle, France) were randomly assigned into three groups of 20 mice each. In the study with H3N8 virus, 5–7-wk-old, 14–18-g (at viral challenge), female BALB/c mice (Charles River Laboratory, Sant'Angelo Lodigiano, Italy) were randomly assigned into four groups of 20 mice each. The mice were housed 10 per cage with high-efficiency particulate air filters (Charles River Laboratory) in biosafety level 2 containment facilities at the Bio Medical Research Center of Alfort National Vet School, Maisons Alfort, France. The mice were fed a sterile rodent maintenance diet (A010-Safe, F89 Augy) and still water (Beaupré). All the studies using live viruses were performed under biosafety level 2 enhanced containment. The animal studies were conducted under applicable laws and guidelines and were compliant with the National Research Council recommendations (34–36). The studies were approved by the Institutional Ethics Committee of Bio Medical Research Center of Alfort National Vet School (no. C2EA-16, from October 2011; Maisons Alfort, France).

Viral challenge. Madin–Darby canine kidney cells were incubated in complete RPMI 1640 medium supplemented with 5% FCS at 37°C in a humidified atmosphere with 5% CO_2. Stocks of the influenza A viruses A/Equi2/Miami/1/63(H3N8) and A/California [A/California/07/2009(H1N1) pandemic] were grown in embryonated hen eggs (F-38 Grenoble; Lohmann Hatcheries) after eventual passages in mice (2 and 0, respectively, for each strain). All strains were obtained by courtesy of the Pasteur Institute Flu Laboratory, Paris, France. Virus stocks were prepared from allantoic fluid and stored in aliquots at −70°C. The viral titers of the Equi2/Miami/1/63 and A/California/07/2009 stocks (3×10^8 PFU/ml and 1.4×10^8 PFU/ml, respectively) were determined by standard plaque assay using Madin–Darby canine kidney cells (37). The infectivity of these viral strains in our mouse model was titrated by intranasal infection with 4-fold serial dilutions of the viruses in Eagle's MEM to determine the LD_{50}, and the challenge dose was adjusted thereafter to the closest multiple of LD_{50} corresponding to the calculated LD_{90} in all experiments. The LD_{50} titers were calculated using the method described by Reed and Muench (38). LD titration of stock virus in 7-wk-old female BALB/c mice was performed by intranasal inoculation of groups of five mice with 40 μl of 4-fold serially diluted virus in PBS (pH 7.2) (Difco Laboratories). Mice were monitored for the development of signs consistent with influenza infection for 7 d and were euthanized if their clinical status met any of the following criteria: loss of 20% of the prechallenge body weight, development of any neurologic or respiratory signs, or an inability to eat or drink.

The mice were challenged intranasally with two LD_{50} equivalents of influenza A/California/07/2009(H1N1) pandemic strain or five LD_{50} of influenza A/Equi2/Miami/1/63(H3N8) strain in 50 μl of sterile saline divided equally between both nostrils. The unchallenged mice received a diluent alone (PBS). The mice were weighed before infection and then every 3 d for the duration of the experiment.

Treatment administration. In H1N1 study, the hd-anti–IFN-γ were administered by gavage twice daily with a 7-h interval between the doses of 0.2 ml/mouse (i.e., 0.4 ml/mouse/d), starting 5 d before and up to 21 d after the challenge, as has been reported previously (19). In parallel to the gavages, the hd-anti–IFN-γ were added in the drinking water at a ratio of 1:3 (changed daily). Taking into account that the mean water uptake of mice is 5.7 ± 0.2 ml/30 g body weight (39) and body weight of mice in this experiment was 18–20 g, the hd-anti–IFN-γ uptake from drinking tank was calculated to be ∼0.903 ml/mouse/d. In H3N8 study, the hd-anti–IFN-γ were administered in the same way but up to 26 d after challenge and without adding to the drinking water. Oseltamivir, which was proven to have antiviral activity against influenza virus within preclinical studies (40, 41), was used as the reference drug. Oseltamivir solution was prepared the day before the challenge by dissolving the contents of 75 mg capsule of Tamiflu (oseltamivir; Roche, Welwyn Garden City, U.K.) in purified water (H1N1 study) or in 0.9% NaCl (H3N8 study) up to concentration of 0.4 mg/ml. Oseltamivir (10 mg/kg/d in H1N1 study or 4 mg/kg/d in H3N8 study) was administered by gavage twice daily with a 7-h interval between the doses either alone (both studies) or in combination with the hd-anti–IFN-γ (in H1N1 study) (i.e., 0.4 ml/mouse/d starting from 1 h to 5 d after the challenge). Five days before the challenge and from day 6 to 21 (H1N1 study) or 26 (H3N8 study) after the challenge, the mice from these groups received water in the same volume but without oseltamivir. The control group of the infected mice received vehicle (drinking water) (0.4 ml/mice/d) using the same dosage regimen as the hd-anti–IFN-γ group. The mice in the control (both studies), in oseltamivir only and in oseltamivir plus hd-anti–IFN-γ (H1N1 study) groups received plain drinking water (replaced daily) in the respective drinking tanks during the experiments.

It should be mentioned that the combination of oseltamivir and the hd-anti–IFN-γ was tested against influenza A [A/California/07/2009(H1N1) pandemic] only. This strain of virus, but not A/Equi2/Miami/1/63(H3N8), was chosen because it was responsible for the swine flu pandemic in 2009–2010.

Testing of the original Abs to IFN-γ was considered not suitable because orally given proteins and peptides (and Abs particularly) typically and

Downloaded from http://www.jimmunol.org/ by guest on October 10, 2021

without specific modifications have extremely low bioavailability in the concentration range of around 0–2% (42, 43). However, oral administration of the diluted protein solutions could decrease the rate of protein proteolysis and accelerate its diffusion through the intestinal mucosa (44).

Therapeutic efficacy of tested treatments in mice. In the survival study, the mice were observed daily for 21 or 26 d postinfection to record the death rate (H1N1 and H3N8 studies, respectively). In H1N1 study, mice were weighted once before (5 d before inoculation) and five times after the challenge (exactly after the challenge and then on days 5, 7, 12, and 19 after inoculation), always after 5.00 PM. In H3N8 study, mice were weighted at least twice a week starting from 10 d before inoculation till 26 d after inoculation, always after 5.00 PM.

Statistical methods

Statistical analysis was performed using SAS 9.4. Descriptive statistics were represented as median, lower and upper quartiles (radioligand binding competition assay), median and interquartile range (ELISpot), mean values for survival (in vivo), and mean and standard deviations for weights (in vivo). Reported p values are adjusted for multiple comparisons. Multiplicity adjustments were performed on analysis of each experiment individually. ELISpot data were analyzed using the exact Wilcoxon test. Radioligand binding competition assay data were analyzed using the exact Wilcoxon test with Dwass–Steel–Critchlow–Fligner multiple comparison procedure. The p value multiplicity adjustment for this data was performed with Holm method (step-down Bonferroni, PROC MULTTEST). H3N8 and H1N1 survival data were analyzed using the log-rank test (PROC LIFETEST) with the Bonferroni adjustment for multiple comparisons. H3N8 and H1N1 weight data were analyzed using a repeated measures ANOVA model (PROC MIXED). Group, day, and group by day interaction factors were included. Applicability conditions of mixed model were assessed using Q–Q plot for residuals. Pairwise comparisons were performed using least-squares means estimates with Holm multiplicity adjustment method.

Results

The hd-anti–IFN-γ induce conformational changes in IFN-γ: ^{1}H NMR spectroscopy

The experimental method of choice to study the influence of hd-anti–IFN-γ on the structural properties of IFN-γ is using high-resolution solution NMR spectroscopy. The advantage of NMR spectroscopy over other protein structure investigation techniques, such as x-ray crystallography and cryogenic electron microscopy, is that it is applied to samples in their aqueous solution environment, and it is possible to detect transient interactions between ligands and proteins (45). The success of protein NMR spectroscopy is based on the fact that chemical shifts of nuclei in a protein are highly susceptible to changes in the local environment of those nuclei. Thus, we can use chemical shifts as reporters for potential structural effects of the hd-anti–IFN-γ on its target, IFN-γ (Fig. 1). Commonly used NMR-active nuclei in proteins include proton and nitrogen. The natural abundance of ^{1}H is 100%, and therefore, proton NMR spectra can be measured with proteins that are not enriched in isotopes (i.e., those that are unlabeled). The one-dimensional (1D) ^{1}H spectrum for unlabeled IFN-γ alone acquired on a 900-MHz spectrometer is shown in Fig. 2. The 1D spectrum gives an overview of the profile of IFN-γ and confirms feasibility of further NMR studies. Water absorbs at 4.7 ppm, with OH protons in its vicinity, whereas chemical shifts to the left (higher parts-per-million values) predominantly arise from NH and aromatic protons, whereas those around 0 ppm arise from aliphatic side chains. Shown in Fig. 2A is the full ^{1}H range, whereas Fig. 2B shows an enlargement of the peptide backbone (NH) containing range. We can see that there is a large number of differences observed between IFN-γ alone (bottom spectra) and IFN-γ, to which the hd-anti–IFN-γ had been added. Several peaks changed their intensities, with new peaks appearing and some peaks missing. Overall, the peaks in the control spectrum are broader and, therefore, less intense, as evidenced by the lower signal-to-noise ratio at the same number of scans. Areas with less signal overlap in the 1D spectrum allow identification of the backbone NH groups of residues E39, W37, and D42 (see labels in Fig. 2B). One can see very clearly how these three peaks change their relative intensity (increase) upon addition of hd-anti–IFN-γ. Thus, the 1D proton NMR spectroscopic analysis of IFN-γ in the presence and absence of the hd-anti–IFN-γ indicates that there are changes in the local environment of a number of peaks in both backbone and side chains of amino acids of the molecule. These changes suggest that there are conformational changes in IFN-γ.

The hd-anti–IFN-γ induce conformational changes in IFN-γ: ^{1}H,^{15}N-HSQC NMR spectroscopy

Because of the expected overlap in 1D proton spectra, only three protons could be assigned in this spectrum (E39, W37, and D42). Resolving the overlap requires increasing the dimensionality and decreasing the number of peaks in an NMR spectrum. This can be accomplished by combining ^{1}H NMR with one or more nuclei, such as carbon or nitrogen, also abundant in proteins. However, the natural abundance of the corresponding NMR-active isotopes are low, and therefore, they need to be enriched in a recombinant system. We therefore expressed IFN-γ in *Escherichia coli* and purified it to enable incorporation of the NMR-active nucleus of nitrogen, ^{15}N. This allows application of a pulse sequence, the HSQC, that selects only those protons connected to another nucleus, and we chose ^{15}N. The smaller number of signals and the second dimension of the spectrum will allow resolving the majority of NH backbone signals of IFN-γ. This has been done previously (32) and we can therefore use the existing assignment of peaks to label all of the cross-peaks in the spectrum. The 2D ^{1}H–^{15}N HSQC spectrum recorded on a 900-MHz NMR spectrometer for IFN-γ alone (blue) and for IFN-γ in the presence of the hd-anti–IFN-γ or placebo (red) is shown in Fig. 3A, 3B, respectively. We were able to assign nearly all of the backbone NH peaks for IFN-γ alone using the prior assignment (32). The spectrum for IFN-γ with the hd-anti–IFN-γ or placebo, respectively, was recorded under the same conditions as for IFN-γ alone except that the concentration of IFN-γ alone was higher, allowing us to collect a larger number of increments in the nitrogen dimension (see *Materials and Methods*). This was necessary to assign all peaks while keeping the sample requirements low to enable the largest possible volume of addition of the hd-anti–IFN-γ or control, respectively. We used placebo as a control, whereas water without the anti–IFN-γ Abs was subjected to the same treatment as the Ab-containing samples. Thus, this control is more stringent than just buffer used in the 1D NMR experiments shown in Fig. 2. The comparison between placebo spectra (recorded under identical conditions as that of the hd-anti–IFN-γ; shown in Fig. 3A) and IFN-γ alone is shown in Fig. 3B.

First, we inspect the spectral changes observed upon addition of the hd-anti–IFN-γ, shown in Fig. 3A. There are many red peaks that are not observed in IFN-γ alone (blue peaks), but they lie outside of the assigned peaks and may correspond to an aggregated conformation that is very different from the conformation for which peaks and structure have been assigned. If we zoom in on the spectrum in the region of assigned peaks, we can see that the centers of red signals are shifted. For example, the change in the peak position of aspartic acid at position 42 corresponds to the change of the local environment for this amino acid, confirming our finding with unlabeled IFN-γ in the 1D proton NMR spectra shown in Fig. 2. The resolution and assignment of many more peaks allowed us to identify a number of additional changes. A total of 13 peaks had shifted after addition of the hd-anti–IFN-γ. The clearly shifted peaks in the IFN-γ plus hd-anti–IFN-γ spectrum were identified as A9, E39, E40, D42, I45, Q47, I50, F82,

Downloaded from http://www.jimmunol.org/ by guest on October 10, 2021

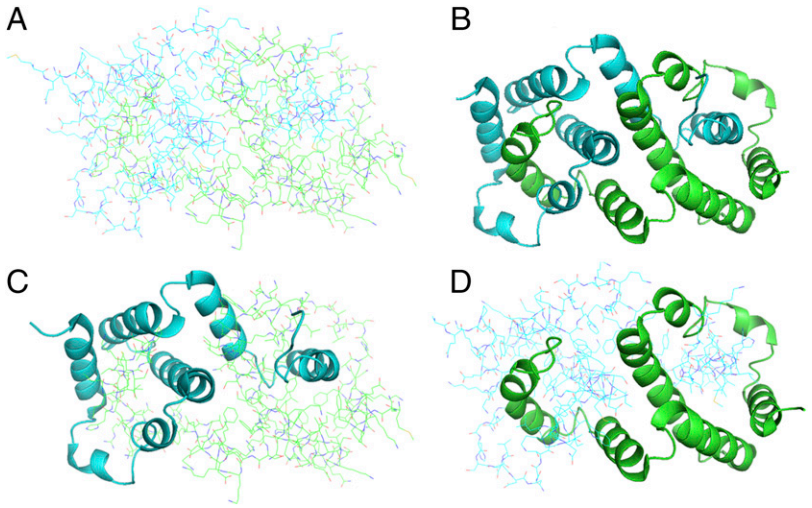

FIGURE 1. Three-dimensional structure of IFN-γ. Protein Data Bank (PDB) identifier (ID) code 1FG9 was used. IFN-γ has 127 aa (aa 0–126). We used the numbering from the PDB file shifted by 1 in referencing residues throughout the manuscript. (**A**) Atomic representation of the IFN-γ dimer. Each monomer is shown in green and turquoise, respectively. (**B**) Secondary structure representation of the IFN-γ dimer. Color coding and view as in (A). (**C**) Secondary structure representation of the turquoise monomer and atomic representation of the green monomer. View as in (A). (**D**) Reverse of (C), with secondary structure representation of the green monomer and atomic representation of the turquoise monomer. View as in (A).

F83, and S85, as well as V117, A119, and E120 at the C terminus (Table I). The corresponding alterations were not observed when the placebo control was added (Fig. 3B).

Superimposition of all the changes in chemical shift parameters that we observed upon addition of the hd-anti–IFN-γ, but not placebo, onto the three-dimensional structure of IFN-γ is shown in Fig. 3C, alongside with the zoomed in regions of the NMR spectra. The different colors indicate the magnitude of chemical shift that we observed. Highest changes are depicted in red and blue, moderate changes in yellow. Pink and greenish colors indicate residues located at the interface between dimers. For comparison, we show as an inset the structure image from Fig. 1 to highlight the positions of the two monomers in the dimer. This comparison reveals that many of the changes are observed at this interface region. Out of 13 residues with shifted peaks, seven are positioned at the dimer interface of IFN-γ: E39, E40, D42, Q47, F82, V117, and A119 (Fig. 3C). Some of the peaks with a major increase in intensity were the ones we already identified in the 1D ^{1}H spectrum of unlabeled IFN-γ: E39, W37, and D42 (Fig. 2B). The three identified peaks with increased intensity upon the hd-anti–IFN-γ treatment are all situated close to the bend between helices B and C at the center of the dimer interface of IFN-γ. The data strongly suggest that there is a change in structure of IFN-γ focused on the interface between the two monomers and, thus, will likely affect the monomer–dimer equilibrium of IFN-γ.

The hd-anti–IFN-γ improves binding of IFN-γ to the IFN-γ receptor

Human monocyte-like cell line U-937 abundantly expresses high-affinity receptor to IFN-γ (46). To verify and quantify highly specific binding of IFN-γ to its receptor on U-937 cells, we performed a competition binding assay. The data indicate that there was a single class of high-affinity binding sites with the binding inhibition constant (*Ki*) equal to 1.1×10^{-9} ($0.1–1 \times 10^{-9}$ reported by van Loon et al. (47) [1991]). The treatment of U-937 cells with the hd-anti–IFN-γ resulted in a significant increase in the specific binding of [^{125}I]IFN-γ to IFN-γ receptor (percentage of specific binding in buffer control) versus both vehicle and hd-anti–TNF-α ($p < 0.05$): 148.92 (148.20; 155.44) versus 119.50 (99.20; 129.64) percentage (vehicle) and 109.11 (73.22; 143.82) percentage (hd-anti–TNF-α).

The hd-anti–IFN-γ stimulate in vitro IFN-γ production by PBMCs

Earlier, we have shown that IFN-γ production was significantly augmented as a result of treating animals with the hd-anti–IFN-γ (48). We used an ELISpot assay to detect and quantify the effects of the hd-anti–IFN-γ on IFN-γ–producing cells in vitro. PBMC were resuspended in a culture medium containing the hd-anti–IFN-γ or vehicle and stimulated with the ICE Peptide Pool. The number of IFN-γ–producing cells in a medium containing the hd-anti–IFN-γ was significantly higher (40 spots [interquartile range = 13]) in comparison with 26 spots [interquartile range = 4] in vehicle [$p < 0.05$]) (Fig. 4). The unstimulated cells in background wells showed no activity (Supplemental Fig. 2).

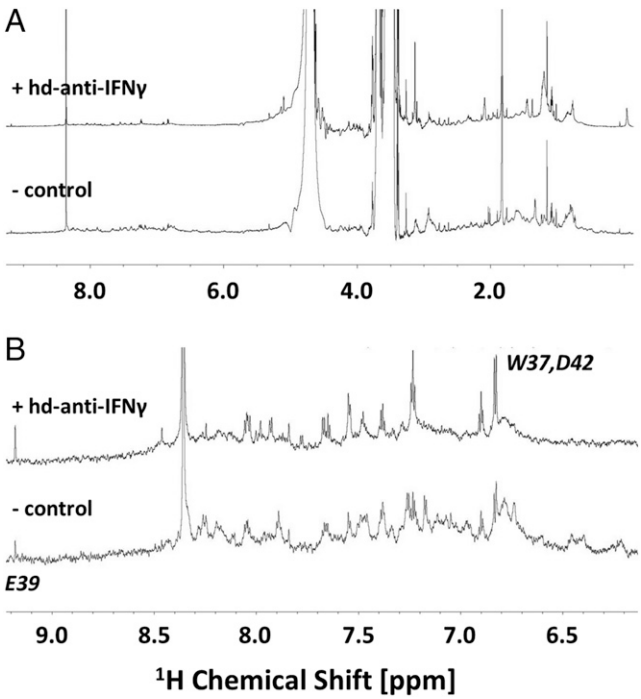

FIGURE 2. 1D NMR spectroscopic analysis of the interaction between the hd-anti–IFN-γ and IFN-γ. Comparison of unlabeled IFN-γ alone, the negative (−) control (bottom spectra, identified as -control) with the sample, unlabeled IFN-γ in the presence of the hd-anti–IFN-γ (top spectra, identified as positive [+] for added hd-anti–IFN-γ). The experiment represents an average of 10,240 scans at 25°C. Water suppression was achieved by excitation sculpting with gradients. (**A**) Full-range proton spectrum showing all protons in the sample. In addition to IFN-γ protons, there are several buffer peaks of high intensity (off scale). (**B**) Zoom-in showing the peptide backbone range.

Downloaded from http://www.jimmunol.org/ by guest on October 10, 2021

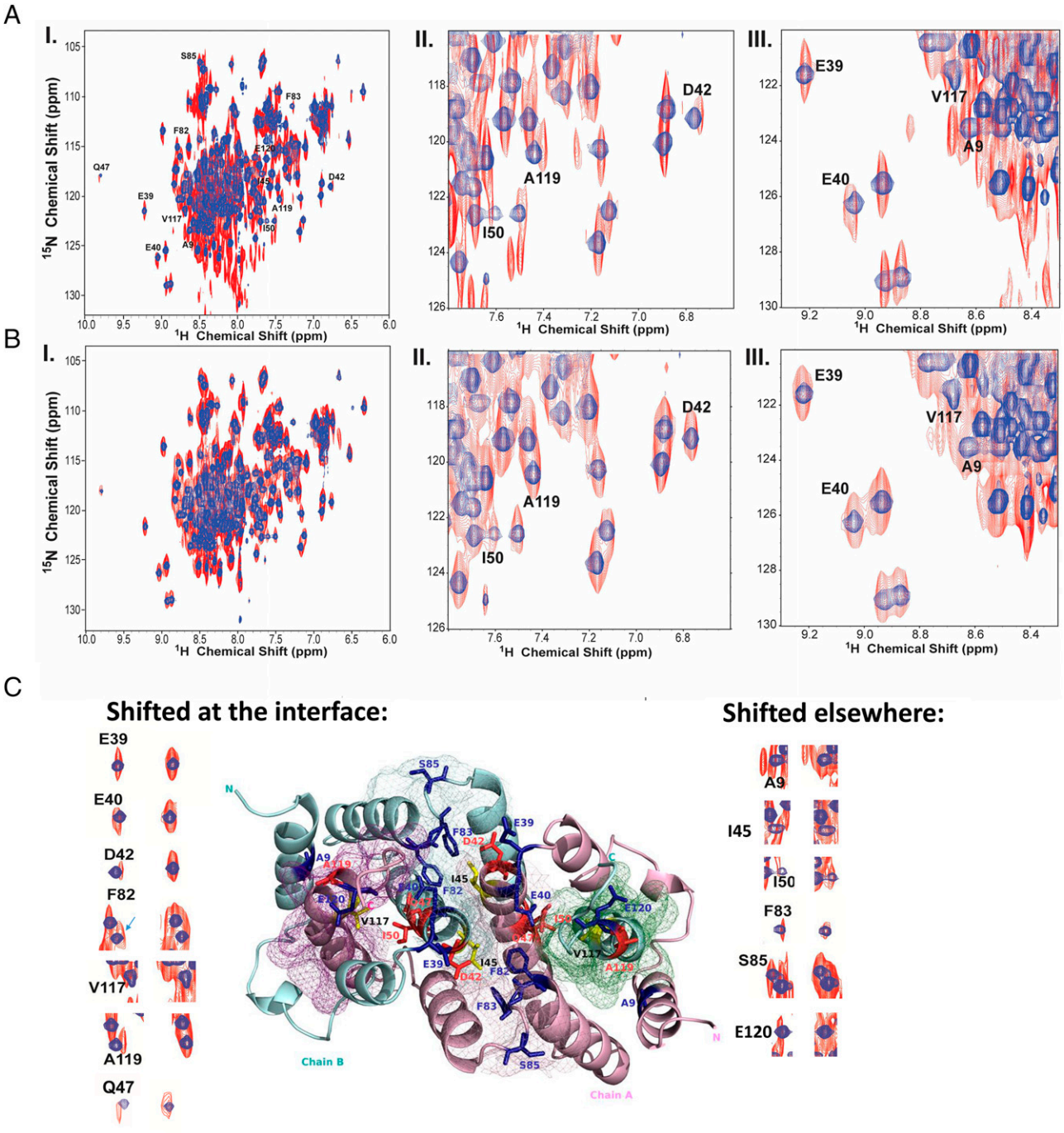

FIGURE 3. 2D NMR spectroscopic analysis of the interaction between the hd-anti–IFN-γ and IFN-γ. (**A**) Overlay of ^{15}N–^{1}H–HSQC spectra of IFN-γ in the absence (blue) or presence (red) of the hd-anti–IFN-γ. The 2D ^{1}H–^{15}N spectra for IFN-γ alone (blue) were acquired with 128 scans in the proton dimension and 128 scans in the nitrogen dimension at 25°C. For NMR samples containing IFN-γ with added highly diluted Abs were acquired with 2048*34 scans (red). (**AI**) Overview of the whole spectrum; (**AII** and **AIII**) expansion of local regions of rhe spectrum shown in AI. (**B**) Overlay of ^{15}N–^{1}H–HSQC spectra of IFN-γ in the absence (blue) or presence (red) of placebo. Data acquisition as in (A). (**C**) Structural mapping of the 13 chemical shift changes observed in IFN-γ upon its interaction with the hd-anti–IFN-γ alongside their expanded regions for each individual residue (note that each residue appears in the image twice because of the dimer formation). The domain-swapped active dimer of IFN-γ is represented as a ribbon diagram in pink (Chain A) and cyan (Chain B) to highlight individual chains. The signals that showed chemical shift changes in the range 0.01–0.02 and 0.02–0.04 ppm are represented as blue and red sticks, respectively (see Table I). Weaker changes were observed for V117 and I45 (yellow sticks, black labels). The corresponding spectra are shown to the left for residues at the dimer interface and on the right for those outside of the interface. Hotspots of interaction are highlighted by mesh (i.e., the dimer interface at the mirror plane of the two monomers and the C-terminal chain interfaces). (**BI**) Overview of the whole spectrum; (**BII** and **BIII**) expansion of local regions of the spectrum shown in BI. The inset shows the same image as in Fig. 1B to help the viewer identify the two monomers in the dimer. View and Protein Data Bank (PDB) identifier (ID) as in Fig. 1.

Downloaded from http://www.jimmunol.org/ by guest on October 10, 2021

Table I. Chemical shift changes in IFN-γ NMR spectra induced by hd-anti–IFN-γ addition

	Peaks That Disappeared or Completely Changed	Residues That Exhibited Shifts (0.01–0.02 ppm)	Residues That Exhibited Maximum Shift (0.02–0.04 ppm)
IFN-γ residue number	I45 and V117	A9, E39, E40, F82, F83, S85, and E120	D42, Q47, I50, and A119

This finding indicates that the hd-anti–IFN-γ participate in regulating IFN-γ levels by enhancing IFN-γ secretion and/or inducing proliferation of IFN-γ–producing cells. Images of the individual plates can be found in the Supplemental Fig. 2.

The hd-anti–IFN-γ increase survival of mice with influenza A infection

BALB/c female mice were inoculated intranasally with either influenza A/H1N1 or A/H3N8 and treated orally with the hd-anti–IFN-γ (starting 5 d before and up to 21 d or 26 d after the challenge, respectively), vehicle (drinking water), the classic antiviral drug oseltamivir (Tamiflu), or a combination of the hd-anti–IFN-γ and oseltamivir (for H1N1). The mortality and body weight were used as endpoints of the study. The animals treated with the hd-anti–IFN-γ exhibited increased survival rates (Fig. 5). The hd-anti–IFN-γ were at least as effective in reducing mortality as oseltamivir alone, with survival rates of 95 versus 75% for H3N8 ($p > 0.05$) and 80 versus 70% for H1N1 ($p > 0.05$), statistically significant difference versus vehicle (20% for H3N8 and 30% for H1N1) was found for each treatment group ($p < 0.05$). The survival rate of combined treatment with the hd-anti–IFN-γ and oseltamivir was 75 versus 70% of oseltamivir alone for H1N1 ($p > 0.05$). At the end of the study, the body weight loss was significantly lower in all treatment groups compared with vehicle group ($p < 0.05$) for H3N8 infection; no significant differences were found for the body weight loss in the groups of animals with H1N1 infection (Fig. 6).

Discussion

In our previous studies, we demonstrated that the biological effects of high dilutions of Abs are very specific. For instance, when we assessed the effects of the in vivo administration of highly diluted biologics on cytokine secretion, we observed that only treatment with the hd-anti–IFN-γ led to the increase of IFN-γ production by murine lymphocytes, whereas the highly diluted Abs to erythropoietin, hd-anti–TNF-α, or placebo exerted no significant effect (48). We also showed that the affinity of Ag–Ab interaction (IFN-γ and Abs to IFN-γ, respectively) was altered in the presence of the hd-anti–IFN-γ (27).

Thus, the specificity of these effects led us to hypothesize that the highly diluted Abs may act directly on the target Ag allosterically, causing conformational changes similar to those sometimes observed during Ab–Ag binding. For example, binding of an Ab to an Ag may induce allosteric effects resulting in the Ag's conformational changes (28). mAbs recognizing human growth hormone were shown to cause allosteric changes in the hormone that affected binding to its receptor and modified the hormone's biological activity (49).

In the current study, we assessed effects of the hd-anti–IFN-γ on the molecular structure and biological functions of IFN-γ. First, we used high-resolution solution NMR spectroscopy to detect any conformational changes in the IFN-γ molecule occurring in the presence of hd-anti–IFN-γ. The mature human IFN-γ is a homodimer of two subunits each composed of 143-aa residues with total molecular mass of 45 kDa (50). The IFN-γ monomer consists of a core of six α-helices and an extended unfolded sequence in the C-terminal region (12, 51). The biologically active dimer is formed by antiparallel interlocking of the two monomers. Addition of the hd-anti–IFN-γ to the IFN-γ sample introduced both global and specific changes in the NMR spectrum. Overall, the intensity and the resolution of the spectrum improved. We found a total of 13 aa that show a change in position or intensity upon addition of the hd-anti–IFN-γ, but not placebo.

Seven of the residues with chemical shift changes in our spectra were assigned to residues located at the dimer interface and including the C terminus of IFN-γ. Fig. 2B clearly shows the sharpening of ^{1}H resonances in IFN-γ upon the addition of hd-anti–IFN-γ. Based on this result and the high dilution of anti–IFN-γ and, thus, low concentrations of hd-anti–IFN-γ, we can rule out the formation of an hd-anti–IFN-γ/IFN-γ complex. Such a large complex would result in very broad peaks because of the high molecular mass of the complex, and it would not be possible to resolve resonances by NMR. Thus, it follows that the observed chemical shifts are due to a transient interaction of IFN-γ with hd-anti–IFN-γ. The observed increase in intensity and sharpness of the resonances and the appearance of new peaks are indicative of a change in the monomer–dimer equilibrium. Because the IFN-γ dimer is formed by domain swapping (see Fig. 1), in which

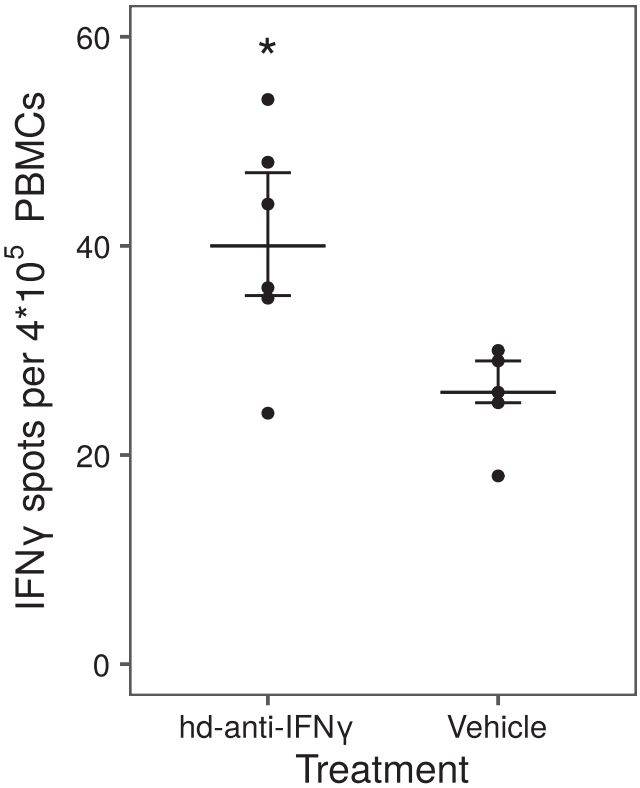

FIGURE 4. Treatment with the hd-anti–IFN-γ enhances IFN-γ production by peptide pool–stimulated PBMCs. ELISpot analysis of IFN-γ–producing cells was performed on human PBMC culture stimulated with the ICE Peptide Pool in the presence of hd-anti–IFN-γ or vehicle. *$p < 0.05$, versus vehicle.

Downloaded from http://www.jimmunol.org/ by guest on October 10, 2021

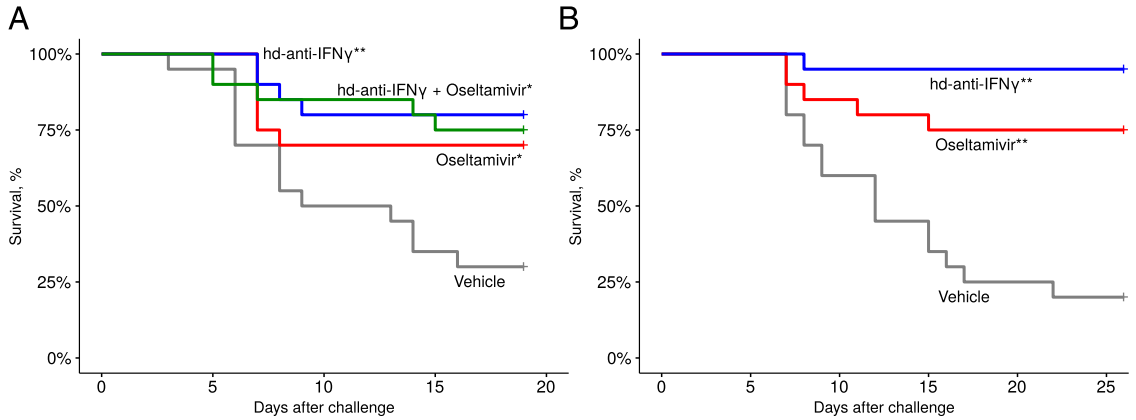

FIGURE 5. The hd-anti–IFN-γ protect female BALB/c mice against influenza A infection (**A**) The hd-anti–IFN-γ exhibited antiviral activity against influenza A [A/California/07/2009(H1N1) pandemic] with efficacy comparable with oseltamivir ($p > 0.05$), as demonstrated by increased survival rates compared with those in the challenged vehicle group ($p < 0.05$). In addition, the hd-anti–IFN-γ in combination with oseltamivir improved antiviral activity of the reference drug ($p > 0.05$). *$p < 0.05$ versus vehicle, **$p < 0.01$ versus vehicle. (**B**) The hd-anti–IFN-γ exhibited antiviral activity against influenza A [A/Equi2/Miami/1/63(H3N8)] with efficacy comparable with oseltamivir ($p > 0.05$), as demonstrated by increased survival rates compared with those in the challenged vehicle group ($p < 0.01$). **$p < 0.01$ versus vehicle.

individual secondary structure elements such as helices are taking the corresponding place in the other structure, the interface is extended over a wide range of the structure, and a change in oligomerization state actually requires at least partial unfolding of the structure. Thus, the most general conclusion we can draw from the changes in chemical shifts observed by NMR spectroscopy is that there is a change in structure of IFN-γ induced by the addition of hd-anti–IFN-γ, with particular emphasis on the dimer interface. Likely, such steric changes in the dimer structure could potentially affect the stability of the dimer, alter oligomerization kinetics of IFN-γ, and influence stoichiometry of the IFN-γ/IFN-γ receptor complex. These are all hypotheses that can be tested in future in-depth studies of oligomerization states and kinetics, as has been done previously for the study of the equilibrium between monomeric, dimeric, and oligomeric states in the absence of hd-anti–IFN-γ (52).

Responses to IFN-γ are activated through its interaction with a high-affinity heterodimeric receptor consisting of IFN-γ receptor 1 (IFNGR1) and IFNGR2. IFN-γ binding to the receptor activates the JAK–STAT pathway. Through its C-terminal region, IFN-γ also binds (but with lower affinity) to the glycosaminoglycan heparan sulfate at the cell surface. This interaction inhibits IFN-γ biological activity as well as possibly protecting it from proteolytic cleavage and regulating tissue targeting and local accumulation (53). Interestingly, intracellular IFN-γ has been reported to possess biological activity without the recognition of the extracellular domain of its high-affinity receptor. It was suggested that a complex consisting of activated Stat1a in association with IFNGR1 undergoes nuclear translocation in the presence of human IFN-γ, as the IFN-γ C-terminal peptide contains a nuclear localization signal (54).

Thus, we next examined if the hd-anti–IFN-γ could alter the ligand–receptor interaction, taking into account that biologically active form of IFN-γ is a dimer (50) and IFN-γ binds to its receptor as a dimer (55). In addition, the C-terminal region of IFN-γ molecule, which exerted spatial changes observed by NMR, plays a critical role in its binding to IFN-γ receptor and IFN-γ signaling (54, 56). The results of the radioligand binding competition assay demonstrated that the hd-anti–IFN-γ enhanced the specific binding of IFN-γ to its receptor.

IFN-γ is a proinflammatory cytokine and is mainly produced by NK, NKT, innate lymphoid cells, $CD4^+$ Th1, and $CD8^+$ CTL and by professional APCs such as macrophages, dendritic cells, and B cells. IFN-γ exerts protective effects through upregulation of cellular immunity, activation of macrophages, and induction of Th1 differentiation. Th1 cells, which secrete IFN-γ, are

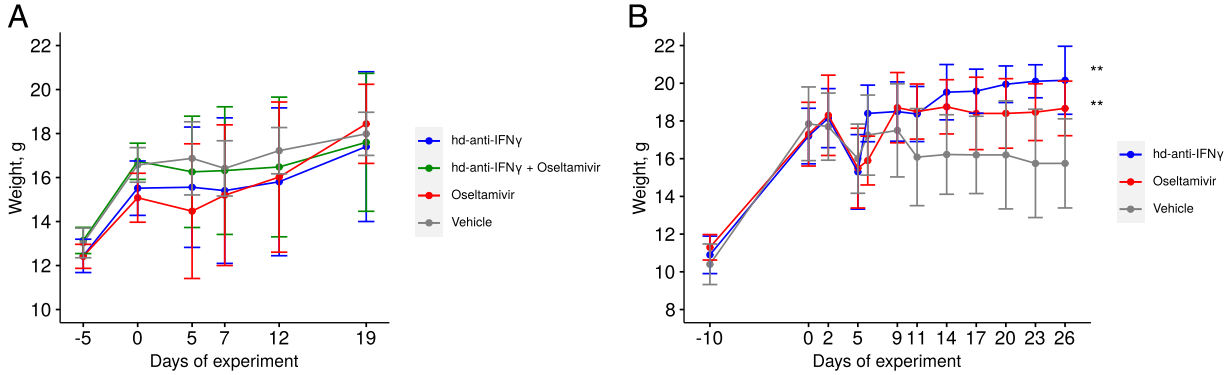

FIGURE 6. The hd-anti–IFN-γ improve weight of female BALB/c mice with influenza A infection. (**A**) The hd-anti–IFN-γ exhibited antiviral activity against influenza A [A/California/07/2009(H1N1) pandemic] with efficacy comparable with oseltamivir ($p > 0.05$), as demonstrated by increased total live weight per treatment group compared with those in the challenged vehicle group. No significant differences were found in total live weight per treatment group compared with those in the challenged vehicle group ($p < 0.05$). (**B**) The hd-anti–IFN-γ exhibited antiviral activity against influenza A [A/Equi2/Miami/1/63(H3N8)] with efficacy comparable with oseltamivir ($p > 0.05$), as demonstrated by increased total live weight per treatment group compared with those in the challenged vehicle group ($p < 0.05$). **$p < 0.01$ versus vehicle.

Downloaded from http://www.jimmunol.org/ by guest on October 10, 2021

promoted tby IFN-γ, IL-12, IL-23, and IL-27 through STAT1, STAT4, and T-bet activation. IFN-γ, IL-12, and IL-27 are part of a positive regulatory feedback loop that enhances the production of these cytokines in the same or different cell types by acting through the cytokine-specific receptors (57). IFN-γ was found to be a powerful upregulatory stimulus for its own gene expression in human PBMC (58). Also, it was shown that the treatment of PBMC with IFN-γ resulted in the secretion of IFN-γ after 24–48 h (59).

To explore the effect of the hd-anti–IFN-γ on IFN-γ production, we treated human PBMCs and measured the number of IFN-γ–secreting cells using an ELISpot assay. We show that the hd-anti–IFN-γ positively regulate viral peptide pool-induced IFN-γ secretion. Possible mechanisms may involve improving the effectiveness of Ag presentation or functional activation of $CD8^+$ cytotoxic T cells. Also, our results might be considered as an indirect evidence of the hd-anti–IFN-γ regulation of positive feedback loop through the activation of the IFN-γ signaling pathway.

IFN-γ plays a critical role in the innate and adaptive immunity against viral and bacterial infections (57). IFN-γ is able to inhibit viral replication directly, but most importantly, the cytokine possesses immunostimulatory and immunomodulatory effects (57). IFN-γ is produced during acute stages of influenza A viral infection and can be detected in the upper respiratory tract secretions and in the serum. However, based on findings in animal models [using injection of neutralizing anti–IFN-γ Abs (60) or IFN-$\gamma^{-/-}$ (61) and IFN-$\gamma R^{-/-}$ (62) mice], it was concluded that control of influenza A infection generally does not depend on IFN-γ. Evasion mechanisms employed by influenza A virus play an important role in this ineffectiveness (63). Interestingly, it was still possible to achieve IFN-γ–specific control of influenza A virus in mouse models. In these cases, animals were either pretreated with IFN inducer polyriboinosinic-polyribocytidylic acid (64) or treated with high doses of IFN-γ at the early stage of infection (65). Thus, pretreatment of animals with the hd-anti–IFN-γ may override resistance of influenza A virus to IFN-γ. In an in vivo study, we examined the hd-anti–IFN-γ antiviral activity against influenza A virus in a mouse model using a 5-d pretreatment protocol. We showed that the hd-anti–IFN-γ was effective against influenza in vivo. These data are in the agreement with our previous reports (19, 22, 23).

Previously, the mechanism of action of a therapeutic drug containing as a main component the highly diluted Abs to the β-subunit of the insulin receptor was studied. We revealed the action of drug on the target molecule (β-subunit of the insulin receptor) (66) and further expanded the research to study the effects at the organismal level (67, 68). In addition, the results of a randomized, placebo-controlled, double-blind clinical trial of this drug efficacy and safety in type 1 diabetes mellitus have been recently published (8).

The results of the current study allow us to conclude that unlike traditional Ab-based drugs, the highly diluted Abs act by inducing conformational modifications in their targets, which then affect interactions of the modified targets with the respective receptors and thus finally orchestrate the target-dependent biological pathway. Highly diluted biologics offer a revolutionary approach for development and clinical application of Ab-based drugs.

Acknowledgments

We thank Christophe Chaumeil and Maria Myslivetc for technical assistance, Alfort National Vet School for murine model guidance, including directions to minimize animal suffering, and members of Euroscreen, S.A., Gosselies, Belgium, for performing experiments with the IFN-γ receptor.

Disclosures

We thank Nicole Mueller and Joan Planas-Iglesias for technical assistance with the preparation of IFN-γ and the structure image in Fig. 3C, respectively. The authors declare the following competing financial interests: OOO "NPF "Materia Medica Holding" sponsored the study, performed statistical analysis, made a decision to publish the work and covered the current article processing charges, and took part in the design of the experiments and the manuscript writing. O.I.E. is a founder, President, and majority shareholder of OOO "NPF "Materia Medica Holding." S.A.T., E.A.G., E.S.D., A.G.E., and A.L.K. are research executives of OOO "NPF "Materia Medica Holding." Different technological versions of the hd-anti–IFN-γ are the substances (single, or one among other components) for commercial drugs Anaferon for children, Anaferon, Ergoferon, and Polyferon produced or produced and marketed by OOO "NPF "Materia Medica Holding." Patents on this substance and the drugs belong to O.I.E. The other authors have no financial conflicts of interest.

References

1. Grilo, A. L., and A. Mantalaris. 2019. The increasingly human and profitable monoclonal antibody market. *Trends Biotechnol.* 37: 9–16.
2. Mahmuda, A., F. K. Bande, K. J. K. Al-Zihiry, N. Abdulhaleem, R. A. Majid, R. A. Hamat, W. O. Abdullah, and Z. Unyah. 2017. Monoclonal antibodies: a review of therapeutic applications and future prospects. *Trop. J. Pharm. Res.* 16: 713–722.
3. Samaranayake, H., T. Wirth, D. Schenkwein, J. K. Räty, and S. Ylä-Herttuala. 2009. Challenges in monoclonal antibody-based therapies. *Ann. Med.* 41: 322–331.
4. Chames, P., M. Van Regenmortel, E. Weiss, and D. Baty. 2009. Therapeutic antibodies: successes, limitations and hopes for the future. *Br. J. Pharmacol.* 157: 220–233.
5. Weiner, G. J. 2015. Building better monoclonal antibody-based therapeutics. *Nat. Rev. Cancer* 15: 361–370.
6. Yanaka, S., Y. Moriwaki, K. Tsumoto, and K. Sugase. 2017. Elucidation of potential sites for antibody engineering by fluctuation editing. *Sci. Rep.* 7: 9597.
7. Epstein, O. 2018. The spatial homeostasis hypothesis. *Symmetry (Basel)* 10: 103.
8. Mkrtumyan, A., T. Romantsova, S. Vorobiev, A. Volkova, N. Vorokhobina, S. Tarasov, M. Putilovskiy, E. Andrianova, and O. Epstein. 2018. Efficacy and safety of Subetta add-on therapy in type 1 diabetes mellitus: the results of a multicenter, double-blind, placebo-controlled, randomized clinical trial. *Diabetes Res. Clin. Pract.* 142: 1–9.
9. Pushkar, D., A. Vinarov, L. Spivak, K. Kolontarev, M. Putilovskiy, E. Andrianova, and O. Epstein. 2018. Efficacy and safety of Afalaza in men with symptomatic benign prostatic hyperplasia at risk of progression: a multicenter, double-blind, placebo-controlled, randomized clinical trial. *Cent. European J. Urol.* 71: 427–435.
10. Rafalsky, V., A. Averyanov, B. Bart, E. Minina, M. Putilovskiy, E. Andrianova, and O. Epstein. 2016. Efficacy and safety of Ergoferon versus oseltamivir in adult outpatients with seasonal influenza virus infection: a multicenter, open-label, randomized trial. *Int. J. Infect. Dis.* 51: 47–55.
11. Krause, C. D., and S. Pestka. 2007. Historical developments in the research of interferon receptors. *Cytokine Growth Factor Rev.* 18: 473–482.
12. Ealick, S. E., W. J. Cook, S. Vijay-Kumar, M. Carson, T. L. Nagabhushan, P. P. Trotta, and C. E. Bugg. 1991. Three-dimensional structure of recombinant human interferon-gamma. *Science* 252: 698–702.
13. Duong, T. T., F. D. Finkelman, B. Singh, and G. H. Strejan. 1994. Effect of anti-interferon-gamma monoclonal antibody treatment on the development of experimental allergic encephalomyelitis in resistant mouse strains. *J. Neuroimmunol.* 53: 101–107.
14. Kaser, A. 2014. Not all monoclonals are created equal - lessons from failed drug trials in Crohn's disease. *Best Pract. Res. Clin. Gastroenterol.* 28: 437–449.
15. Skurkovich, B., and S. Skurkovich. 2003. Anti-interferon-gamma antibodies in the treatment of autoimmune diseases. *Curr. Opin. Mol. Ther.* 5: 52–57.
16. Caruso, A., and A. Turano. 1997. Natural antibodies to interferon-gamma. *Biotherapy* 10: 29–37.
17. Epstein, O. I. 2009. *Ultra-Low Doses (History of One Study).* Publishing House of RAMN, Moscow, Russia, p. 302.
18. Don, E., N. van der Meide, V. Egorov, M. Putilovskiy, and S. Tarasov. 2020. The level of natural autoantibodies to IFN-gamma in varicella infection treated with antiviral drug Anaferon for children: a pilot study. *Immunol. Lett.* 222: 90–94.
19. Don, E. S., A. G. Emelyanova, N. N. Yakovleva, N. V. Petrova, M. V. Nikiforova, E. A. Gorbunov, S. A. Tarasov, S. G. Morozov, and O. I. Epstein. 2017. Dose-dependent antiviral activity of released-active form of antibodies to interferon-gamma against influenza A/California/07/09(H1N1) in murine model. *J. Med. Virol.* 89: 759–766.
20. Zaplatnikov, A. L., B. M. Blokhin, N. A. Geppe, E. G. Kondyurina, A. V. Sukalo, and T. N. Voytovich. 2019. An international multicenter study of release-active antibodies against interferon gamma for flu and acute respiratory viral infections in children. *RMJ. Medical Review* 8: 18–24.
21. Blokhin, B. M., O. V. Shamsheva, N. L. Chernaya, I. G. Sitnikov, S. G. Lazareva, N. B. Balzerovich, O. A. Perminova, O. V. Zhiglinskaya, and M. Yu. Koshavtseva. 2019. Results of a multicentre double-blind placebo-controlled randomized trial of

Downloaded from http://www.jimmunol.org/ by guest on October 10, 2021

the liquid form of Anaferon for children in the treatment of acute upper respiratory tract infections. *Ros Vestn Perinatol i Pediatr* 64: 105–113.
22. Shishkina, L. N., A. N. Sergeev, A. S. Kabanov, M. O. Skarnovich, N. K. Evtin, N. A. Mazurkova, A. A. Sergeev, M. V. Belopolskaya, I. A. Kheyfets, J. L. Dugina, et al. 2008. Study of efficiency of therapeutic and preventive anaferon (pediatric formulation) in mice with influenza infection. *Bull. Exp. Biol. Med.* 146: 763–765.
23. Shishkina, L. N., M. O. Skarnovich, A. S. Kabanov, A. A. Sergeev, S. E. Olkin, S. A. Tarasov, M. V. Belopolskaya, S. A. Sergeeva, O. I. Epstein, E. M. Malkova, et al. 2010. Antiviral activity of Anaferon (pediatric formulation) in mice infected with pandemic influenza virus A(H1N1/09). *Bull. Exp. Biol. Med.* 149: 612–614.
24. Ryzhkina, I. S., L. I. Murtazina, Yu. V. Kiseleva, and A. I. Konovalov. 2015. Self-organization and physicochemical properties of aqueous solutions of the antibodies to interferon gamma at ultrahigh dilution. *Dokl. Phys. Chem.* 462: 110–114.
25. Bunkin, N. F., A. V. Shkirin, N. V. Penkov, S. N. Chirikov, P. S. Ignatiev, and V. A. Kozlov. 2019. The physical nature of mesoscopic inhomogeneities in highly diluted aqueous suspensions of protein particles. *Phys. Wave Phenom.* 27: 102–112.
26. Chikramane, P. S., D. Kalita, A. K. Suresh, S. G. Kane, and J. R. Bellare. 2012. Why extreme dilutions reach non-zero asymptotes: a nanoparticulate hypothesis based on froth flotation. *Langmuir* 28: 15864–15875.
27. Don, E., O. Farafonova, S. Pokhil, D. Barykina, M. Nikiforova, D. Shulga, A. Borshcheva, S. Tarasov, T. Ermolaeva, and O. Epstein. 2016. Use of piezoelectric immunosensors for detection of interferon-gamma interaction with specific antibodies in the presence of released-active forms of antibodies to interferon-gamma. *Sensors (Basel)* 16: 96.
28. Roguin, L. P., and L. A. Retegui. 2003. Monoclonal antibodies inducing conformational changes on the antigen molecule. *Scand. J. Immunol.* 58: 387–394.
29. Directive, E. U. 2004. Directive 2004/27/EC of the European Parliament and of the Council of 31 March 2004 amending directive 2001/83/EC on the community code relating to medicinal products for human use. Available at: https://ec.europa.eu/health/sites/health/files/files/eudralex/vol-1/dir_2004_27/dir_2004_27_en.pdf. Accessed: July 17, 2020.
30. Epshtein, O. I., M. B. Shtark, and T. M. Kolyadko, inventors; O. I. Epshtein, assignee. Method of treating a pathological syndrome and a pharmaceutical agent. United States patent 8,535,664. 2013 Sep 17.
31. Johnson, B. A. 2004. Using NMRView to visualize and analyze the NMR spectra of macromolecules. *Methods Mol. Biol.* 278: 313–352.
32. Grzesiek, S., H. Döbeli, R. Gentz, G. Garotta, A. M. Labhardt, and A. Bax. 1992. 1H, 13C, and ^{15}N NMR backbone assignments and secondary structure of human interferon-gamma. *Biochemistry* 31: 8180–8190.
33. Motulsky, H., GraphPad Software. 1995. GraphPad guide to analyzing radioligand binding data. GraphPad Software, San Diego, CA. Available at: http://fisbio.biof.ufrj.br/restrito/bioEstatistica/90_top_especiais/radiolig.pdf. Accessed: July 17, 2020.
34. Council, N. R. 2010. *Guide for the Care and Use of Laboratory Animals*, 8th Ed. National Academies Press, Washington, DC.
35. Directive 2010/63/EU of the European Parliament and of the Council of September 22, 2010 on the protection of animals used for scientific purposes. 2010. Available at: https://eur-lex.europa.eu/legal-content/EN/TXT/?uri=celex%3A32010L0063 Accessed: July 17, 2020.
36. Kilkenny, C., W. J. Browne, I. C. Cuthill, M. Emerson, and D. G. Altman. 2010. Improving bioscience research reporting: the ARRIVE guidelines for reporting animal research. *PLoS Biol.* 8: e1000412.
37. Rimmelzwaan, G. F., M. Baars, E. C. Claas, and A. D. Osterhaus. 1998. Comparison of RNA hybridization, hemagglutination assay, titration of infectious virus and immunofluorescence as methods for monitoring influenza virus replication in vitro. *J. Virol. Methods* 74: 57–66.
38. Reed, L. J., and H. Muench. 1938. A simple method of estimating fifty percent endpoints. *Am. J. Hyg.* 27: 493–497.
39. Bachmanov, A. A., D. R. Reed, G. K. Beauchamp, and M. G. Tordoff. 2002. Food intake, water intake, and drinking spout side preference of 28 mouse strains. *Behav. Genet.* 32: 435–443.
40. Leneva, I. A., E. I. Burtseva, S. B. Yatsyshina, I. T. Fedyakina, E. S. Kirillova, E. P. Selkova, E. Osipova, and V. V. Maleev. 2016. Virus susceptibility and clinical effectiveness of anti-influenza drugs during the 2010-2011 influenza season in Russia. *Int. J. Infect. Dis.* 43: 77–84.
41. Smee, D. F., M. H. Wong, K. W. Bailey, and R. W. Sidwell. 2006. Activities of oseltamivir and ribavirin used alone and in combination against infections in mice with recent isolates of influenza A (H1N1) and B viruses. *Antivir. Chem. Chemother.* 17: 185–192.
42. Muheem, A., F. Shakeel, M. A. Jahangir, M. Anwar, N. Mallick, G. K. Jain, M. H. Warsi, and F. J. Ahmad. 2016. A review on the strategies for oral delivery of proteins and peptides and their clinical perspectives. *Saudi Pharm. J.* 24: 413–428.
43. Reilly, R. M., R. Domingo, and J. Sandhu. 1997. Oral delivery of antibodies. Future pharmacokinetic trends. *Clin. Pharmacokinet.* 32: 313–323.
44. Valuev, I. L., L. K. Starosel'tseva, L. I. Valuev, G. A. Sytov, M. V. Ul'yanova, L. V. Vanchugova, Yu. A. Talyzenkov, and N. A. Plate. 2007. The physical nature of mesoscopic inhomogeneities in highly diluted aqueous suspensions of protein particles. *Appl. Biochem. Microbiol.* 43: 102–104.
45. Wishart, D. 2005. NMR spectroscopy and protein structure determination: applications to drug discovery and development. *Curr. Pharm. Biotechnol.* 6: 105–120.
46. Rashidbaigi, A., H. F. Kung, and S. Pestka. 1985. Characterization of receptors for immune interferon in U937 cells with 32P-labeled human recombinant immune interferon. *J. Biol. Chem.* 260: 8514–8519.
47. van Loon, A. P., L. Ozmen, M. Fountoulakis, M. Kania, M. Haiker, and G. Garotta. 1991. High-affinity receptor for interferon-gamma (IFN-gamma), a ubiquitous protein occurring in different molecular forms on human cells: blood monocytes and eleven different cell lines have the same IFN-gamma receptor protein. *J. Leukoc. Biol.* 49: 462–473.
48. Epstein, O. I., E. Y. Sherstoboev, A. V. Martyushev-Poklad, Y. L. Dugina, S. A. Sergeeva, and A. M. Dygai. 2004. Dose-dependent effects and specificity of action of antibodies to endogenous regulators in ultralow doses. *Bull. Exp. Biol. Med.* 137: 460–462.
49. Roguin, L. P., R. C. Aguilar, and L. A. Retegui. 1995. Monoclonal antibodies to human growth hormone modulate its biological properties. *Mol. Immunol.* 32: 399–405.
50. Boteva, R., T. Zlateva, V. Dorovska-Taran, A. J. Visser, R. Tsanev, and B. Salvato. 1996. Dissociation equilibrium of human recombinant interferon gamma. *Biochemistry* 35: 14825–14830.
51. Walter, M. R., W. T. Windsor, T. L. Nagabhushan, D. J. Lundell, C. A. Lunn, P. J. Zauodny, and S. K. Narula. 1995. Crystal structure of a complex between interferon-gamma and its soluble high-affinity receptor. *Nature* 376: 230–235.
52. Zlateva, T., R. Boteva, B. Salvato, and R. Tsanev. 1999. Factors affecting the dissociation and aggregation of human interferon gamma. *Int. J. Biol. Macromol.* 26: 357–362.
53. Lortat-Jacob, H. 2006. Interferon and heparan sulphate. *Biochem. Soc. Trans.* 34: 461–464.
54. Ahmed, C. M., M. A. Burkhart, M. G. Mujtaba, P. S. Subramaniam, and H. M. Johnson. 2003. The role of IFNgamma nuclear localization sequence in intracellular function. *J. Cell Sci.* 116: 3089–3098.
55. Krause, C. D., E. Mei, J. Xie, Y. Jia, M. A. Bopp, R. M. Hochstrasser, and S. Pestka. 2002. Seeing the light: preassembly and ligand-induced changes of the interferon gamma receptor complex in cells. *Mol. Cell. Proteomics* 1: 805–815.
56. Subramaniam, P. S., M. G. Mujtaba, M. R. Paddy, and H. M. Johnson. 1999. The carboxyl terminus of interferon-gamma contains a functional polybasic nuclear localization sequence. *J. Biol. Chem.* 274: 403–407.
57. Schoenborn, J. R., and C. B. Wilson. 2007. Regulation of interferon-gamma during innate and adaptive immune responses. *Adv. Immunol.* 96: 41–101.
58. Hardy, K. J., and T. Sawada. 1989. Human gamma interferon strongly upregulates its own gene expression in peripheral blood lymphocytes. *J. Exp. Med.* 170: 1021–1026.
59. Di Marzio, P., P. Puddu, L. Conti, F. Belardelli, and S. Gessani. 1994. Interferon gamma upregulates its own gene expression in mouse peritoneal macrophages. *J. Exp. Med.* 179: 1731–1736.
60. Baumgarth, N., and A. Kelso. 1996. In vivo blockade of gamma interferon affects the influenza virus-induced humoral and the local cellular immune response in lung tissue. *J. Virol.* 70: 4411–4418.
61. Graham, M. B., D. K. Dalton, D. Giltinan, V. L. Braciale, T. A. Stewart, and T. J. Braciale. 1993. Response to influenza infection in mice with a targeted disruption in the interferon gamma gene. *J. Exp. Med.* 178: 1725–1732.
62. Nicol, M. Q., G. M. Campbell, D. J. Shaw, I. Dransfield, Y. Ligertwood, P. M. Beard, A. A. Nash, and B. M. Dutia. 2019. Lack of IFNγ signaling attenuates spread of influenza A virus in vivo and leads to reduced pathogenesis. *Virology* 526: 155–164.
63. Hale, B. G., R. A. Albrecht, and A. García-Sastre. 2010. Innate immune evasion strategies of influenza viruses. *Future Microbiol.* 5: 23–41.
64. Wong, J. P., E. G. Saravolac, D. Sabuda, H. B. Levy, and M. Kende. 1995. Prophylactic and therapeutic efficacies of poly(IC.LC) against respiratory influenza A virus infection in mice. *Antimicrob. Agents Chemother.* 39: 2574–2576.
65. Weiss, I. D., O. Wald, H. Wald, K. Beider, M. Abraham, E. Galun, A. Nagler, and A. Peled. 2010. IFN-gamma treatment at early stages of influenza virus infection protects mice from death in a NK cell-dependent manner. *J. Interferon Cytokine Res.* 30: 439–449.
66. Gorbunov, E. A., J. Nicoll, E. V. Kachaeva, S. A. Tarasov, and O. I. Epstein. 2015. Subetta increases phosphorylation of insulin receptor β-subunit alone and in the presence of insulin. *Nutr. Diabetes* 5: e169.
67. Bailbé, D., E. Philippe, E. Gorbunov, S. Tarasov, O. Epstein, and B. Portha. 2013. The novel oral drug Subetta exerts an antidiabetic effect in the diabetic Goto-Kakizaki rat: comparison with rosiglitazone. *J. Diabetes Res.* 2013: 763125.
68. Kheyfets, I. A., A. A. Spasov, M. P. Voronkova, J. L. Dugina, and O. I. Epstein. 2012. Study of hypoglycemic activity of Subetta and rosiglitazone on the model of streptozotocin-induced diabetes mellitus in rats. *Bull. Exp. Biol. Med.* 153: 54–56.

Downloaded from http://www.jimmunol.org/ by guest on October 10, 2021